Subsets of cortico-cortical evoked potentials propagate as traveling waves

Justin M. Campbell[1,2,3], Tyler S. Davis[3], Daria Nesterovich Anderson[7], Amir Arain[4], Cory S. Inman[2,5], Elliot H. Smith[2,3], John D. Rolston[6,8]

[1]MD-PhD Program, School of Medicine, [2]Interdepartmental Program in Neuroscience, and Departments of [3]Neurosurgery, [4]Neurology, [5]Psychology, and [6]Biomedical Engineering, University of Utah, Salt Lake City, UT, USA

[7]School of Biomedical Engineering, Faculty of Engineering, University of Sydney, Sydney, New South Wales, Australia

[8]Department of Neurosurgery, Brigham & Women's Hospital, Harvard Medical School, Boston, MA, USA

Corresponding Author:

Justin M. Campbell

Department of Neurosurgery

Clinical Neurosciences Center

University of Utah

175 N Medical Drive East

Salt Lake City, UT, 84132

Email: justin.campbell@hsc.utah.edu

Disclosures:

JDR has received consulting fees from Medtronic, NeuroPace, and Corlieve Therapeutics.

Keywords:

- Traveling wave; CCEP; epilepsy

Abbreviations:

iEEG, intracranial electroencephalography; SEEG, stereoelectroencephalography; CCEP, cortico-cortical evoked potential; SOZ, seizure onset zone

ORCID:

Justin M. Campbell: 0000-0002-8685-2081

Tyler S. Davis: 0000-0001-8823-6189

Daria Nesterovich Anderson: 0000-0002-9093-7504

Amir Arain: 0000-0003-0572-0552

Cory Inman: 0000-0003-2928-6252

Elliot H. Smith: 0000-0003-4323-4643

John D. Rolston: 0000-0002-8843-5468

Abstract

Emerging evidence suggests that the temporal dynamics of cortico-cortical evoked potentials (CCEPs) may be used to characterize the patterns of information flow between and within brain networks. At present, however, the spatiotemporal dynamics of CCEP propagation cortically and subcortically are incompletely understood. We hypothesized that CCEPs propagate as an evoked traveling wave emanating from the site of stimulation. To elicit CCEPs, we applied single-pulse stimulation to stereoelectroencephalography (SEEG) electrodes implanted in 21 adult patients with intractable epilepsy. For each robust CCEP, we measured the timing of the maximal descent in evoked local field potentials and broadband high-gamma power (70-150 Hz) envelopes relative to the distance between the recording and stimulation contacts using three different metrics (i.e., Euclidean distance, path length, geodesic distance), representing direct, subcortical, and transcortical propagation, respectively. Many evoked responses to single-pulse electrical stimulation appear to propagate as traveling waves (~17-30%), even in the sparsely sampled, three-dimensional SEEG space. These results provide new insights into the spatiotemporal dynamics of CCEP propagation.

Introduction

Cortico-cortical evoked potentials (CCEPs) provide rich insights into the structural and functional organization of the brain.[1] These responses to direct electrical stimulation have been used for many different applications—for example, mapping distinct types of connectivity[2–4], quantifying signal complexity across levels of consciousness[5–8], and tracking the effects of stimulation on neural plasticity.[9,10] Thus, CCEPs may be a valuable tool for extracting causal information about large-scale brain networks and their spatiotemporal dynamics.[11]

Recent studies have investigated the temporal properties of CCEPs, characterizing the relationship between the amplitude and latency of the early N1 component (10-50ms) and axonal conduction delays resulting from the underlying white matter architecture.[12–14] For example, a recent study that combined CCEPs with tractography observed considerable age-related changes in the transmission speed of cortico-cortical signals.[15]

Emerging evidence suggests that the temporal dynamics of CCEPs may also provide novel insights into the patterns of information flow between and within brain networks.[16,17] At present, these spatiotemporal dynamics of CCEP propagation cortically and subcortically are incompletely understood. We hypothesized that CCEPs propagate as an evoked traveling wave, analogous to what we previously observed in interictal epileptiform discharges (IEDs).[18]

Neural traveling waves are electrical perturbations that propagate across the brain with non-zero phase lag.[19] These traveling waves are thought to play a role in neural communication and cortical computation across a range of spontaneous and stimulus-evoked phenomena.[20–26] Their precise role in these processes is unknown; however, the development of technologies for recording distributed neural activity with high resolution has enabled new empirical approaches for investigating their sources and functional properties.[27–29] We thus sought to leverage

intracranial recordings in humans, an approach that provides excellent temporal resolution and spatial precision, to determine whether single-pulse electrical stimulation would elicit CCEPs that propagated as a traveling wave from the site of stimulation.

Methods

Participants

Twenty-one adult patients with medically intractable epilepsy (n = 7 female) underwent intracranial monitoring with stereoelectroencephalography (SEEG) to localize their seizure foci (**Table 1**). We performed stimulation mapping while patients were off their antiseizure medications during their inpatient hospital stay. Results from some of these stimulation sessions were reported in prior studies of evoked potential recordings.[30,31] All patients provided informed consent prior to participation, and our team took care to implement the recommended principles and practices for ethical intracranial neuroscientific research.[32] The study was approved by the University of Utah Institutional Review Board (protocol #00069440).

Electrode localization and registration

To localize electrodes, we co-registered each patient's pre-operative magnetization-prepared rapid gradient-echo (MP-RAGE), fluid-attenuated inversion recovery (FLAIR), or T1 MRI to their post-operative CT using custom MATLAB software and the *Statistical Parametric Mapping Toolbox* (SPM 12; https://www.fil.ion.ucl.ac.uk/spm/software/spm12/). Automated image processing, electrode detection, and anatomical localization of intracranial electrodes were performed using the open-source *Locate electrodes Graphical User Interface* (LeGUI; https://github.com/Rolston-Lab/LeGUI) software[31] and Brainnetome atlas.[33]

Specific properties of CCEPs differ between areas within the seizure onset zone (SOZ) compared to areas outside the SOZ (e.g., early evoked high-frequency activity).[34–37] To control for these differences, electrode contacts inside and outside the SOZ were analyzed separately—a board-certified epileptologist identified and designated epileptogenic regions based on seizure semiology, imaging, and electrophysiological recordings.

Electrophysiological recordings and stimulation

Neurophysiological data were recorded from intracranial SEEG electrodes with variable contact spacing (Ad-Tech Corp., Racine, WI; DIXI Medical, France) using a 128-channel neural signal processor (Neuroport, Blackrock Microsystems, Salt Lake City, UT) and sampled at 1kHz. In line with recommended practices, we chose an intracranial electrode in the white matter with minimal artifact and epileptiform activity as the online reference.[38] Stimulation was delivered using a 96-channel neurostimulator (Cerestim, Blackrock Microsystems, Salt Lake City, UT).

CCEP mapping consisted of monopolar single-pulse electrical stimulation (biphasic, 5.0-7.5 mA, 500 ms pulse width) administered to a subset of electrodes in a randomly selected order every 2.5-3.5 s over an ~45 min session.[30] Each electrode contact received between 4-50 discrete trials of single pulse electrical stimulation; variability in trial count across contacts stemmed from time constraints and clinical considerations (i.e., emphasis on hypothesized seizure foci).

Signal processing

Intracranial recordings were first divided into pre-stimulation and post-stimulation epochs (-1000 to -5 ms and 5-1000 ms, respectively), with stimulation onset set at time zero. Peri-stimulation data (-5 to 5 ms) was removed to mitigate stimulation artifacts. Next, data were

bandpass filtered at 0.3-250 Hz and re-referenced offline to the common median across channels to minimize noise.[39]

We measured the broadband, high-gamma power (70-150 Hz) envelope from local field potentials recorded during the post-stimulation epochs to characterize the spectrotemporal response to single pulses of electrical stimulation. Specifically, we bandpass filtered the post-stimulation data using a zero-phase fourth-order Butterworth filter, applied the Hilbert transform, and multiplied the result by its complex conjugate.

CCEP detection

Fundamental considerations in the detection and analysis of CCEPs have been reviewed previously.[1,30,40,41] Numerous methods for CCEP detection have been employed in prior studies, including amplitude thresholding[42], machine-learning frameworks analyzing evoked response shapes[43], stimulation-induced gamma-based network identification (SIGNI)[44], and others.[45]

In this study, evoked responses were considered CCEPs if (1) the trial median of the early response period (5-100 ms post-stimulation) contained ≥ 15 ms of continuous values more than threefold greater than the median (across time and trial) of the immediate pre-stimulation epoch (-100 to -5 ms) and (2) the median (across time and trial) of the early response period (5-100 ms post-stimulation) was > 30 μV, as previously described.[30] Responses measured from contacts located within white matter were excluded. Evoked responses that did not meet these criteria were not designated as robust CCEPs and were excluded from subsequent analyses.

Distance

We used three distinct distance metrics to capture subcortical and cortical traveling waves in the 3D SEEG space: Euclidean distance, path length, and geodesic distance (**Figure 1**). These metrics were chosen to ensure accurate distances between electrode contacts and to compare biologically plausible metrics (i.e., path length, geodesic distance) against naïve approaches which do not account for the brain's unique geometry (i.e., Euclidean distance).

Euclidean. The Euclidean distance between each electrode pair is defined by the length of the shortest line segment connecting the two electrode locations in 3D space. Accordingly, we calculated the pairwise 3D Euclidean distance between all possible contacts using the following:

$$d = \sqrt{(x_1 - x_2)^2 + (y_1 - y_2)^2 + (z_1 - z_2)^2}$$

where x_n, y_n, and z_n correspond to the 3D anatomical coordinates of the electrode contact within the patient's brain (normalized to MNI space).

Path length. Path length, which approximates signal propagation via axonal pathways, is the average distance between two electrodes derived from patient-specific tractography. Diffusion-weighted imaging (DWI) was acquired for all patients as part of standard clinical care. Using the *FMRIB* Software Library (FSL), DWI images were eddy corrected, and a network connectivity matrix was generated using network mode in the *probtractx2* function.[46,47] A volume with a 0.5 cm radius at each electrode centroid was used as the seed region, and segmentation was computed in *FreeSurfer*.[48] Finally, the output N x N network matrix, which corresponds to average tractographic distances between each combination of N number of contacts, was made symmetric.

Geodesic. Geodesic distance, which approximates signal propagation through the cortex, is the distance along the cortical surface between two electrodes. Cortical surface segmentations for each hemisphere were generated within *FreeSurfer* using each patient's structural MRI.[48]

Using these surfaces, the geodesic distance was calculated with the *SurfDist* python package (v 0.15.5, https://pypi.org/project/surfdist/). Electrodes were excluded from the distance calculation if that electrode's centroid was more than 1 cm from the nearest cortical surface. The geodesic distance was calculated between each electrode pair on the same hemisphere.

Traveling wave analyses

To characterize CCEP propagation, we adapted methods used to previously define the velocity and direction of traveling waves evoked by IEDs.[18] For each CCEP identified, we determined the time at which the evoked response was most rapidly decreasing (i.e., maximal descent, MD), using:

$$MD = \text{argmin}_t\left(\frac{\Delta L(t)}{\Delta t}\right)$$

Where L represents the CCEP local field potential amplitude or high-gamma power. Max descent was chosen, among other possible CCEP features (e.g., N1/N2 peaks), because our prior research validated the feature as a computationally efficient and robust predictor for traveling wave analyses.[49]

For each contact stimulated, we regressed the distance between the stimulation contact and the contact(s) where robust CCEPs were recorded onto their respective trial-averaged max descent timing. A stimulation contact was determined to evoke a traveling wave if a significant linear relationship between distance and max descent timing was observed ($p < 0.05$); to control for false positives, we performed 1000-fold permutation testing against a null distribution of shuffled distances (**Figure 2**). Only the linear models which survived permutation testing were considered traveling waves. The propagation velocity of traveling waves was obtained from the slope of the linear model and converted to m/s to facilitate comparison with what has been

reported previously. We used the *seaborn* library[50] to fit a Gaussian kernel density estimate to the traveling wave velocities and model R^2 values to visualize their distributions (**Figure 3B-C**).

Statistical analyses

We performed a series of Anderson-Darling tests for normality[51], which determined that non-parametric statistical tests were most appropriate. Accordingly, we used Wilcoxon signed-rank tests to compare traveling wave proportions across patients and Kolmogorov-Smirnov tests to compare traveling wave velocities and R^2 distributions between distance metrics. To identify proportional differences in the number of traveling waves observed across areas, we performed a series of chi-squared tests for independence followed by false discovery rate correction to control for false positives.[52] Chi-squared tests were also used to test for proportional differences in the number of traveling waves evoked by stimulation of electrodes inside vs. outside the SOZ.

Results

The demographics and clinical characteristics of the patient cohort are shown in **Table 1**. Following SEEG monitoring, SOZs were defined in 18/21 (85.71%) of patients, most commonly in the mesial temporal lobe (55.56%). On average, 10.95% of the SEEG electrodes were located within the SOZ.

Across all patients, we recorded from 1,015 intracranial electrode contacts (48.33 ± 17.61 per patient, mean ± SD). We administered a total of 17,541 trials of single pulse electrical stimulation (835.29 ± 420.22 per patient) to 914 intracranial electrode contacts (43.52 ± 19.05 per patient). Summary statistics for the stimulation experiments are shown in **Table 2**.

Traveling waves were frequently observed from analyses of CCEP amplitude max descent using each of the three distance metrics: Euclidean (EUC), path length (PL), and geodesic (GEO). Across all patients, traveling waves measured with EUC, PL, and GEO were observed in 24.47% (± 17.54), 19.00% (± 15.82), and 12.70% (± 15.09) of channels stimulated, respectively. At the level of individual patients, traveling waves measured with EUC were more common than PL ($W = 16.00$, $p < 0.01$), PL was more common than GEO ($W = 53.50$, $p < 0.05$), and EUC was more common than GEO ($W = 19.50$, $p < 0.01$) (**Supplemental Figure 1**).

Since stimulation was applied to areas distributed throughout the brain, we sought to characterize regional differences in the frequency of evoked traveling waves. The electrode localization and registration pipeline identified stimulated electrodes located in 20 distinct regions (**Supplemental Table 1**). Our chi-square tests showed significant differences in the proportion of traveling waves evoked from stimulation of the amygdala (Amyg), hippocampus (Hipp), and middle frontal gyrus (MFG) relative to other brain regions with EUC (Amyg: $\chi^2(1,914) = 12.53$, $p < 0.01$; Hipp: $\chi^2(1, 914) = 7.76$, $p < 0.05$; MFG: $\chi^2(1, 914) = 7.84$, $p < 0.05$), and for the hippocampus and cingulate gyrus (CG) with PL (Hipp: $\chi^2(1, 914) = 17.39$, $p < 0.001$; CG: $\chi^2(1, 914) = 8.93$, $p < 0.05$). No regional differences were observed for models using GEO ($p > 0.05$) (**Figure 3A**). We did not observe any difference in the frequency or velocity of traveling waves evoked from stimulation inside vs. outside the SOZ ($p > 0.05$).

We observed a median traveling wave propagation velocity of 1.07 (± 0.55) m/s, 3.15 (± 2.42) m/s, and 2.18 (± 1.23) m/s for the models using EUC, PL, and GEO, respectively (**Figure 3B**). Comparisons of the traveling wave velocity distributions were significantly different between each distance metric, with EUC > GEO > PL (EUC vs. GEO: $D = 0.475$, $p < 0.001$; EUC vs. PL: $D = 0.713$, $p < 0.001$; GEO vs. PL: 0.364, $p < 0.001$). We observed that linear

models using EUC and PL as distance metrics explained a greater proportion of variance (R^2) than those using GEO (EUC vs. GEO: $D = 0.142$, $p < 0.05$, PL vs. GEO: $D = 0.145$, $p < 0.05$) (**Figure 3C**), suggesting CCEPs are more likely to propagate via subcortical axons, rather than via surface conduction.

To ensure that our method for traveling wave identification wasn't limited to the choice of CCEP amplitude as a feature, we applied the same analyses using stimulation-evoked broadband high-gamma power (70-150 Hz). Using this alternative approach, a similar pattern of results emerged: traveling waves measured with EUC, PL, and GEO were observed in 30.12% (± 16.92), 22.52% (± 17.29), and 17.29% (± 14.30) of channels stimulated, respectively. At the level of individual patients, traveling waves measured with EUC were more common than PL ($W = 20.00$, $p < 0.01$), and EUC was more common than GEO ($W = 11.00$, $p < 0.001$). There was no significant difference between the number of traveling waves measured with PL and GEO ($p > 0.05$). (**Supplemental Figure 2**). Traveling waves were observed more frequently when high-gamma max descent was used rather than amplitude max descent for EUC ($W = 41.00$, $p < 0.05$) and GEO ($W = 34.50$, $p < 0.01$) but not PL ($W = 36.00$, $p = 0.17$).

The median time to max descent in the CCEPs was 39.0 ms (± 34.54) and 26.0 ms (± 44.07) for evoked amplitude and high-gamma power, respectively. Max descent timings across the two measures of amplitude and high-gamma power were positively correlated [$r(13577) = 0.31$ ($p < 0.001$)] (**Figure 4**).

Discussion

We applied single-pulse electrical stimulation to intracranial SEEG electrodes in a cohort of patients with intractable epilepsy to study the spatiotemporal dynamics of CCEP propagation.

In doing so, we observed a subset of CCEPs that propagate as traveling waves and exhibit similar characteristics to traveling waves observed in spontaneous and task-evoked activity.

The range of propagation velocities we observed (0.16-7.59 m/s) was comparable to those reported previously for mesoscopic (0.1-0.8 m/s) and macroscopic traveling waves (1-10 m/s)–consistent with the axonal conduction velocities of unmyelinated and myelinated white matter fibers within the cortex, respectively.[19] Large-scale network models suggest that neural traveling waves emerge spontaneously from these axonal conduction delays.[53] Similar traveling wave velocities have also been reported from observations of IEDs[18] and spontaneous neocortical alpha and theta oscillations.[24] Additionally, a recent study that leveraged biologically informed modeling of CCEPs and tractography from patients in the F-TRACT database (f-tract.eu) reported a median cortico-cortical axonal conduction velocity of 3.9 m/s[14], a value very close to what we observed in our PL models of traveling waves propagation along white matter tracts: 3.15 m/s (± 2.42).

We recorded traveling waves in ~17-30% of the channels stimulated, depending on the metrics used. In contrast, task-evoked traveling waves previously observed in spatially clustered alpha and theta oscillations appear 2-3x more frequently.[21,24] There are several reasons why stimulation-evoked traveling waves may not have been observed more ubiquitously. For one, we utilized SEEG recordings, which inherently provide a limited representation of 3D volumes since contacts along the same lead are arranged linearly. Thus, spatial sampling tends to be sparse relative to surface electrocorticographic electrodes.[54] Subsequent investigation of traveling wave dynamics in high-density electrocorticographic recordings may offer superior spatial resolution at the meso- and macroscale. Additionally, since the shape of CCEP responses can be highly

variable, metrics like max descent may fail to generalize to less stereotypical response shapes, limiting the number of traveling waves observed.

Methodological constraints aside, the observation that only a subset of CCEPs exhibit traveling wave characteristics raises an interesting question: Are spatiotemporal delays in CCEP propagation a possible means of separating biologically-plausible evoked responses from spurious signals? Volume conduction, for example, is a commonly observed artifact in evoked responses to stimulation that confounds the interpretation of CCEPs.[55] With our approach, volume-conducted signals are easily distinguished from genuine traveling waves because they lack a robust, linear relationship between CCEP max descent and electrode distance. Although not the focus of this study, further characterization of CCEPs as a multiregional response may provide novel, clinically relevant insights for the mapping of epileptogenic networks.[56]

Robust CCEPs were most often observed near the stimulation site, adjacent to the stimulating electrode, or along the same lead. These closely spaced electrodes may be best characterized by Euclidean distance, which could explain why this metric led to a higher frequency of traveling waves relative to path length or geodesic distance, metrics which are more biologically plausible paths for subcortical and cortical traveling wave propagation. Interestingly, the models using Euclidean distance or tractographic path length as metrics explained more variance than those using geodesic distance. This suggests that stimulation-evoked traveling waves are better modeled via subcortical axonal propagation rather than surface conduction. Thus, subsequent analysis of the spatiotemporal dynamics of CCEP propagation may benefit from the inclusion of patient-specific tractography.

Our comparison of the regional differences in the response to stimulation suggests that stimulation of certain areas may be more likely to elicit CCEPs that propagate as a robust

traveling wave. The significant areas identified—the hippocampus, amygdala, middle frontal gyrus, and cingulate gyrus—represent intimately connected hub regions; previous studies have reported that single pulse stimulation of these areas tends to elicit robust, broadly distributed CCEPs.[57–59] Prior studies have observed traveling waves in areas throughout the human neocortex.[24] Given that medial temporal lobe structures tend to be oversampled relative to other brain regions, the increased electrode density may have some relationship to the regional differences in stimulation-evoked traveling waves that we observed.

Surprisingly, we did not observe differences in the frequency or speed of traveling waves evoked by stimulation inside vs. outside the SOZ. However, our comparisons focused on the effects of stimulation inside vs. outside the SOZ—a detailed comparison of evoked responses recorded from inside vs. outside the SOZ, which have been shown to exhibit different characteristics[34–37], was not performed.

Numerous studies have established a connection between evoked broadband high-gamma and neuronal population activity.[44] The supplementary analyses of stimulation-evoked broadband high-gamma power allowed for characterization of the spectrotemporal dynamics of CCEPs and provided a distinct but concomitant feature for validating our methodological approach. With both approaches, we observed statistically significant stimulation-evoked traveling waves. These results suggest that this approach to traveling wave detection is robust and that our observations are not simply an artifact of data processing.

The study has a few noteworthy limitations. First, electrode locations are determined solely by clinical considerations, leading to heterogeneity between patients and a denser sampling of regions known to be highly epileptogenic (e.g., mesial temporal lobe). Our prior work on traveling waves was performed using Utah electrode arrays, which have the advantage

of a grid-like orientation, allowing a more straightforward characterization of the spatiotemporal dynamics of traveling wave propagation.

Although max descent is a validated measure for traveling wave analyses[49], it reduces the entirety of the CCEP to a single, discrete measurement with respect to time. Other statistical approaches that leverage the high sampling rate of continuous time-series recordings (e.g., phase-based analyses) have been used in prior studies of endogenous traveling waves [25,60] and may similarly yield novel insights for the analysis of stimulation-evoked traveling waves. We chose the former approach, given that phase-based analyses are less appropriate for non-oscillatory traveling waves.

Finally, we restricted the max descent window to 5-150 ms post-stimulation for our analyses. This window was chosen to include the first downward deflection typically observed in our population of CCEPs. In other studies, this has been referred to as N1 (10-50 ms) or the early negative deflection of the slower N2 (50-200 ms) component. When these separate components are observable, recent evidence suggests they may represent intra- and internetwork communication, respectively.[16] Other analyses have shown that morphological characteristics of evoked waveforms, outside the traditional N1/N2 paradigm, may offer more powerful insights into the anatomy underlying the observed CCEPs.[43] Subsequent studies of stimulation-evoked traveling waves may benefit from analyzing the evoked responses from these two components separately.

Conclusions

Our analyses of CCEPs revealed that many evoked responses to single-pulse electrical stimulation appear to propagate as traveling waves. The stimulation-evoked traveling waves we

observed were robust across multiple distinct methods of identification and exhibited characteristics in line with what has been reported previously with spontaneous traveling waves. Traveling waves were observed across distributed brain areas but were most frequently evoked when stimulating highly connected hub regions (e.g., hippocampus, amygdala). These results highlight previously uncharacterized spatiotemporal dynamics of signal propagation in response to stimulation.

Acknowledgments

Figure 1B was created with BioRender.

Funding

JMC was supported by the National Institute of Neurological Disorders and Stroke (T32 NS115723). JDR was supported by an NIH/NINDS career development award (K23NS114178). DNA was supported by an NIH/NINDS award (F32NS114322). CSI was supported by an NIH/NIMH R01 (R01MH120194) and NSF Foundations Grant (NSF2124252).

Table 1. Demographics and clinical characteristics of the patient cohort.

Patient ID	**Age** (yrs.)	**Sex**	**SOZ**
P1	25.45	M	Bilateral mesial temporal lobe
P2	25.86	M	None identified
P3	35.28	F	Right hippocampus
P4	44.34	M	Right hippocampus
P5	42.36	F	Right OFC
P6	42.21	F	None identified
P7	35.59	F	Right MFG
P8	45.01	M	None identified
P9	41.65	F	Bilateral mesial temporal lobe
P10	29.05	F	Bilateral mesial temporal lobe
P11	33.20	M	Left temporal
P12	27.51	M	Right OFC
P13	22.73	M	Right mesial temporal
P14	54.03	M	Right PVNH
P15	30.29	M	Left mesial temporal
P16	29.76	M	Left frontal operculum
P17	59.61	M	Left temporal
P18	43.17	M	Bilateral hippocampi
P19	45.08	F	Left hippocampus
P20	26.50	M	Bitemporal
P21	37.74	M	Bilateral hippocampi

OFC = orbitofrontal cortex, MFG = middle frontal gyrus, PVNH = periventricular nodular heterotopia.

Table 2. Summary statistics for stimulation experiments.

Patient ID	**Electrodes** (no.)	**Stimulated** (no., %)	**SPES** (no.)	**EUC TWs** (no., %)	**PL TWs** (no., %)	**GEO TWs** (no., %)	**EUC TWs (HG)** (no., %)	**PL TWs (HG)** (no., %)	**GEO TWs (HG)** (no., %)
P1	56	56 (100%)	448	47 (80.4%)	45 (80.4%)	37 (66.1%)	47 (83.9%)	45 (80.4%)	37 (66.1%)
P2	97	94 (96.9%)	940	38 (40.4%)	18 (19.1%)	15 (16.0%)	42 (44.7%)	31 (33.0%)	17 (18.1%)
P3	81	81 (100%)	648	18 (22.2%)	5 (6.2%)	15 (18.5%)	30 (37.0%)	3 (3.7%)	18 (22.2%)
P4	69	69 (100%)	966	11 (15.9%)	3 (4.3%)	17 (24.6%)	17 (24.6%)	3 (4.3%)	10 (14.5%)
P5	48	48 (100%)	480	11 (22.9%)	7 (14.6%)	5 (10.4%)	17 (35.4%)	10 (20.8%)	10 (20.8%)
P6	54	54 (100%)	540	13 (24.1%)	13 (24.1%)	10 (18.5%)	23 (42.6%)	19 (35.2%)	13 (24.1%)
P7	28	24 (85.7%)	240	1 (4.2%)	4 (16.7%)	1 (4.2%)	3 (12.5%)	6 (25.0%)	4 (16.7%)
P8	52	52 (100%)	520	7 (13.5%)	7 (13.5%)	10 (19.2%)	18 (34.6%)	8 (15.4%)	14 (26.9%)
P9	30	23 (76.7%)	1150	2 (8.7%)	3 (13.0%)	0 (0.0%)	7 (30.4%)	3 (13.0%)	2 (8.7%)
P10	39	28 (71.8%)	1400	6 (21.4%)	5 (17.9%)	2 (7.1%)	17 (60.7%)	16 (57.1%)	4 (14.3%)
P11	40	36 (90.0%)	1800	9 (25.0%)	6 (16.7%)	8 (22.2%)	13 (36.1%)	9 (25.0%)	10 (27.8%)
P12	46	38 (82.6%)	1634	14 (36.8%)	13 (34.2%)	12 (31.6%)	11 (28.9%)	13 (34.2%)	9 (23.7%)
P13	48	44 (91.7%)	880	12 (27.3%)	10 (22.7%)	9 (20.5%)	17 (38.6%)	10 (22.7%)	18 (40.9%)
P14	20	20 (100%)	600	2 (10.0%)	2 (10.0%)	0 (0.0%)	0 (0.0%)	1 (5.0%)	2 (10.0%)
P15	40	32 (80.0%)	960	7 (21.9%)	7 (21.9%)	1 (3.1%)	3 (9.4%)	3 (9.4%)	5 (15.6%)
P16	49	43 (87.8%)	1161	14 (32.6%)	12 (27.9%)	2 (4.7%)	12 (27.9%)	12 (27.9%)	4 (9.3%)
P17	36	31 (86.1%)	930	7 (22.6%)	7 (22.6%)	0 (0.0%)	7 (22.6%)	5 (16.1%)	1 (3.2%)
P18	34	34 (100%)	374	1 (2.9%)	3 (8.8%)	0 (0.0%)	9 (26.5%)	13 (38.2%)	2 (5.9%)
P19	42	39 (92.9%)	780	18 (46.2%)	14 (35.9%)	1 (2.6%)	10 (25.6%)	10 (25.6%)	3 (7.7%)
P20	55	38 (69.1%)	760	12 (31.6%)	6 (15.8%)	3 (7.9%)	20 (52.6%)	9 (23.7%)	4 (10.5%)
P21	51	30 (58.8%)	330	20 (66.7%)	6 (20.0%)	3 (10.0%)	12 (40.0%)	4 (13.3%)	2 (6.7%)

SPES = single-pulse electrical stimulation, EUC = Euclidean, PL = path length, GEO = geodesic, TWs = traveling waves, HG = high gamma max descent.

Figure Captions

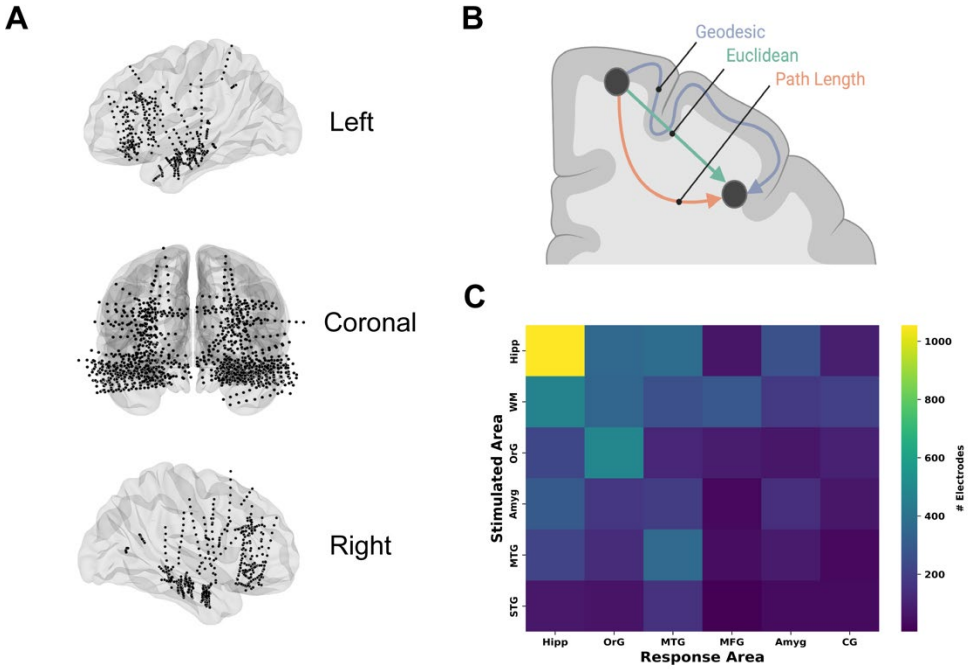

Fig 1. Electrode contact locations and distance metrics. **A.** Brain images depicting SEEG electrode locations across all patients (n = 21 patients). **B.** Schematic comparison of distance measurements between two hypothetical electrode locations. Euclidean distance (teal) represents the shortest straight-line distance between two points. Path length (orange) represents the shortest distance between two points along a diffusion MRI tractography map. Geometric distance (blue) represents the shortest distance between two points along a path restricted within the cortex. **C.** Heatmap of the five areas most frequently stimulated (y-axis) and five areas with the greatest overall number of recorded CCEPs (x-axis) across participants. Tiles are colored by the number of electrodes in the response area with CCEPs evoked by the stimulated area (range 34-1055). Hipp = hippocampus, WM = white matter, OrG = orbitofrontal gyrus, Amyg = amygdala, MTG = middle temporal gyrus, STG = superior temporal gyrus, MFG = middle frontal gyrus, CG = cingulate gyrus.

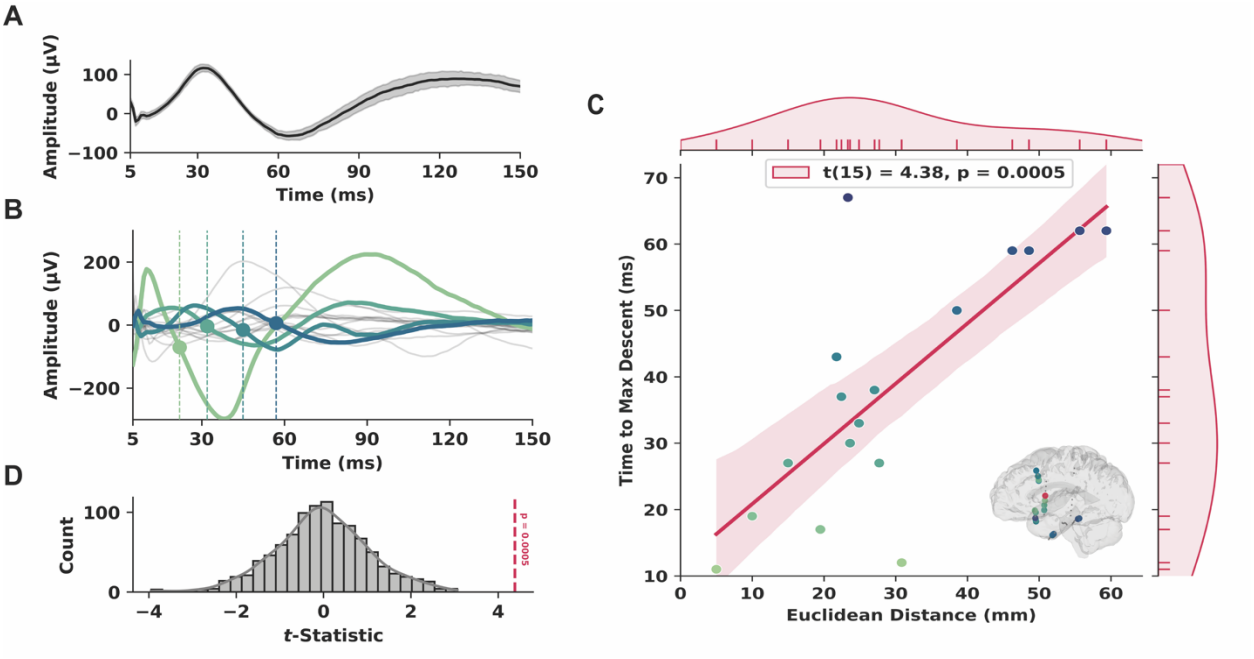

Fig 2. Traveling wave identification. **A.** Example CCEP evoked by single-pulse electrical stimulation. **B.** Subset of CCEPs with amplitude max descents marked. Stimulation at this location evoked robust CCEPs in several other electrodes, some of which are highlighted to show variability in max descent time (indicated with a circle and dotted line). **C.** Example traveling wave. The distance (Euclidean shown) between electrodes was linearly regressed onto max descent time to identify traveling waves. Dots represent electrodes with robust CCEPs, colored by time to max descent (green → blue, early → late). The shaded area represents 95% CI. Brain image shows the location of contacts in the model. **D.** Example 1,000-fold permutation test comparing linear model *t*-values against a null distribution.

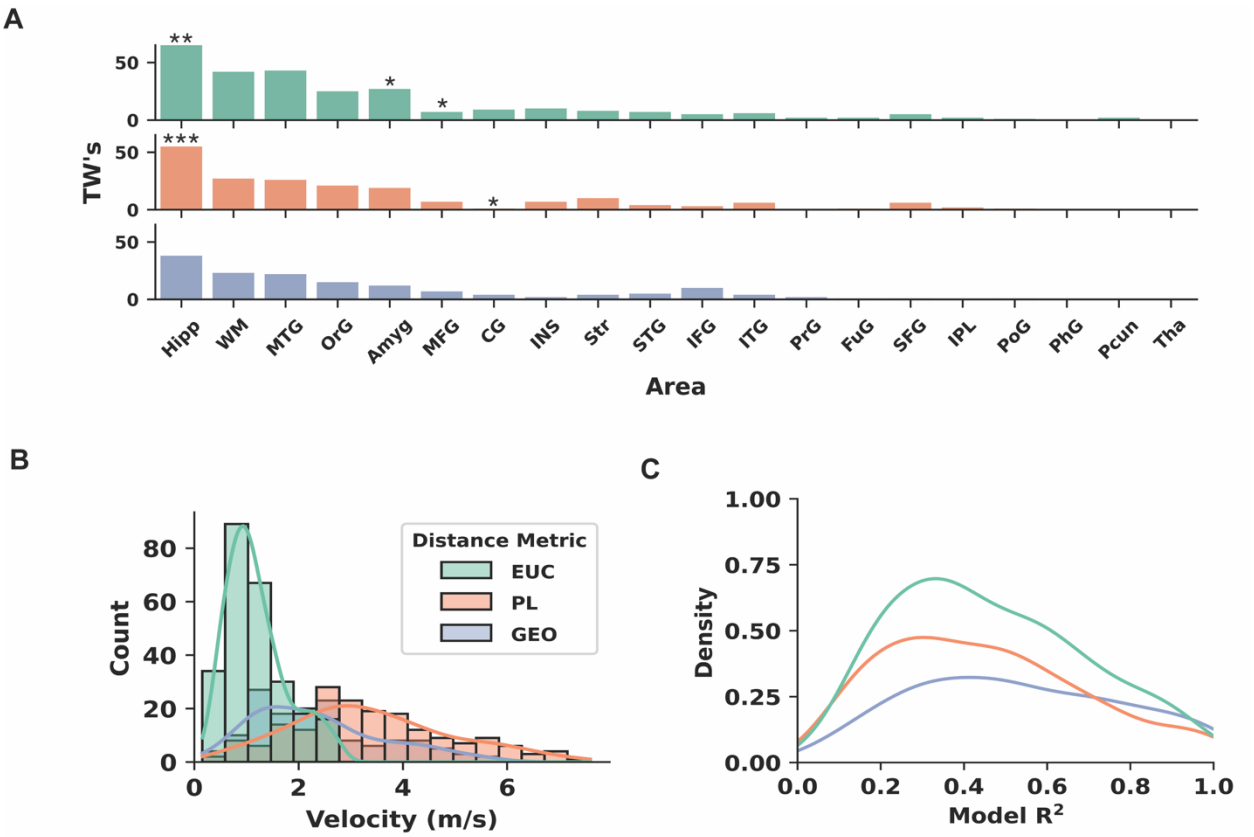

Fig 3. Comparison of CCEP traveling wave stimulation area, speed, and model fit across distance metrics (EUC = Euclidean, PL = path length, GEO = geodesic). **A.** Comparison of the number of electrodes stimulated in each area which elicited a traveling wave. A chi-squared test for independence was performed to compare the relative proportions within each area relative to all others (* = $p < 0.05$, ** = $p < 0.01$, *** = $p < 0.001$). **B.** Histogram of the observed traveling wave speeds. **C.** Kernel-density estimate of the observed linear model R^2 values.

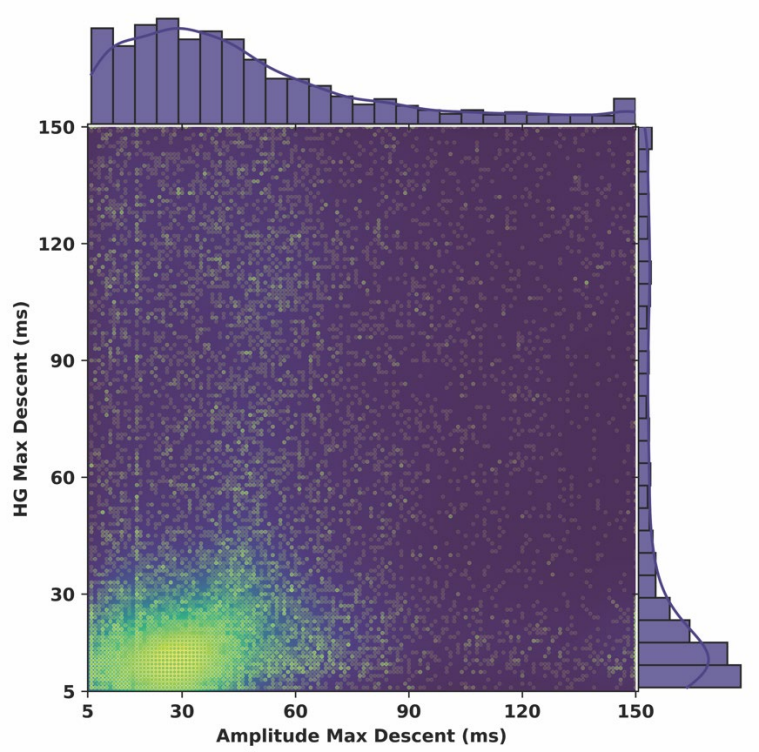

Fig 4. Scatterplot of evoked amplitude and high-gamma (70-150 Hz) max descent times. Histograms along axes show the distribution of values observed.

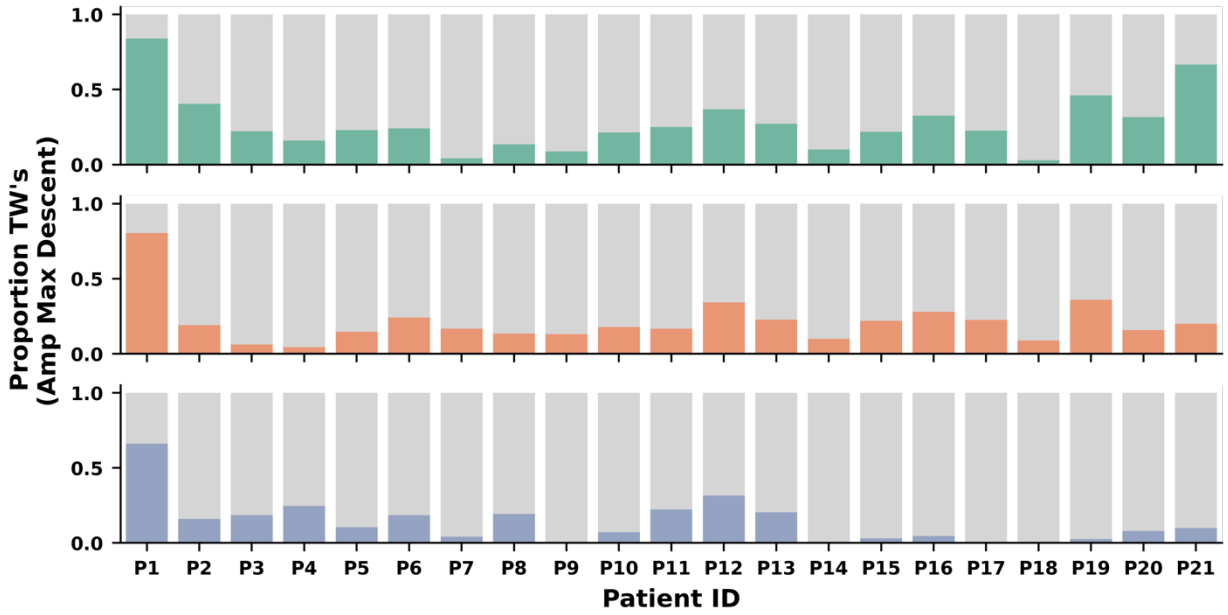

Supplemental Fig 1. The proportion of traveling waves (TWs) observed across 21 patients using Euclidean distance (teal), path length (orange), and geodesic distance (blue) as metrics regressed onto amplitude max descent.

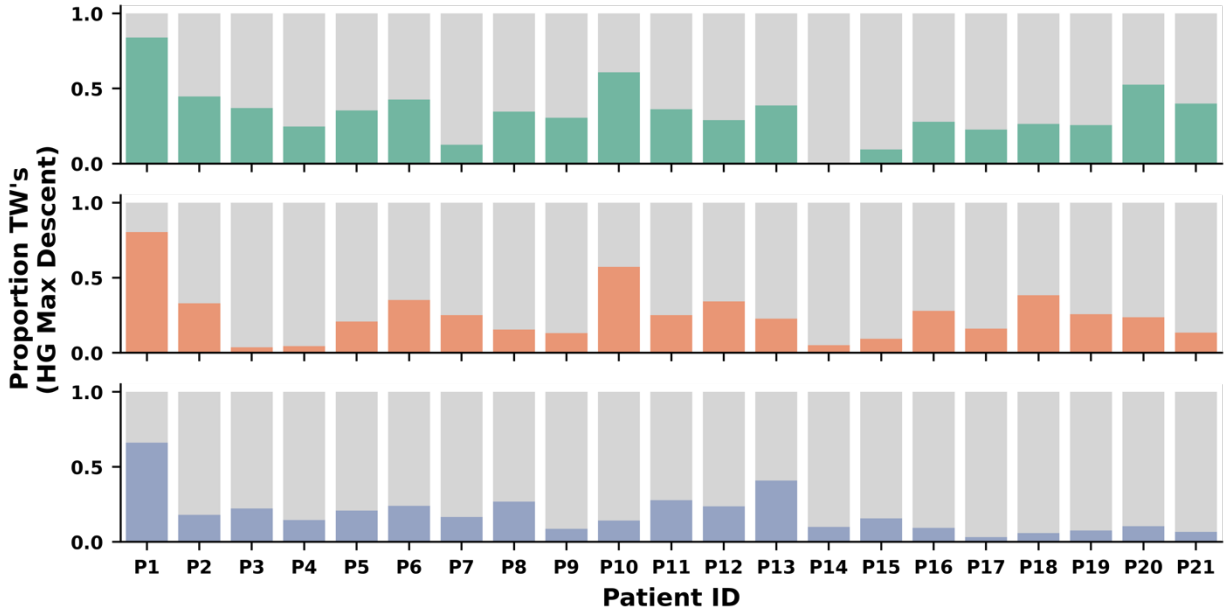

Supplemental Fig 2. The proportion of traveling waves (TWs) observed across 21 patients using Euclidean distance (teal), path length (orange), and geodesic distance (blue) as metrics regressed onto broadband high-gamma (70-150 Hz) max descent.

Supplemental Table 1. The number of unique electrodes stimulated in each area.

Area	**Electrodes** (no.)
Hipp	162
WM	139
MTG	120
OrG	104
Amyg	58
MFG	57
CG	44
INS	39
Str	37
STG	36
IFG	34
ITG	21
PrG	13
FuG	11
SFG	10
IPL	10
PoG	8
PhG	4
Pcun	4
Tha	3

Hipp = hippocampus, WM = white matter, MTG = middle temporal gyrus, OrG = orbitofrontal gyrus, Amyg = amygdala, MFG = middle frontal gyrus, CG = cingulate gyrus, INS = insula, Str = striatum, STG = superior temporal gyrus, IFG = inferior frontal gyrus, ITG = inferior temporal gyrus, PrG = precentral gyrus, FuG = fusiform gyrus, SFG = superior frontal gyrus, IPL = inferior parietal lobule, PoG = postcentral gyrus, PhG = parahippocampal gyrus, Pcun = precuneus, Tha = thalamus.

References

1. Keller CJ, Honey CJ, Mégevand P, Entz L, Ulbert I, Mehta AD. Mapping human brain networks with cortico-cortical evoked potentials. *Philosophical Transactions Royal Soc B Biological Sci*. 2014;369(1653):20130528. doi:10.1098/rstb.2013.0528
2. Keller CJ, Honey CJ, Entz L, et al. Corticocortical Evoked Potentials Reveal Projectors and Integrators in Human Brain Networks. *J Neurosci*. 2014;34(27):9152-9163. doi:10.1523/jneurosci.4289-13.2014
3. Entz L, Tóth E, Keller CJ, et al. Evoked effective connectivity of the human neocortex. *Hum Brain Mapp*. 2014;35(12):5736-5753. doi:10.1002/hbm.22581
4. Crocker B, Ostrowski L, Williams ZM, et al. Local and distant responses to single pulse electrical stimulation reflect different forms of connectivity. *Neuroimage*. 2021;237:118094. doi:10.1016/j.neuroimage.2021.118094
5. Comolatti R, Pigorini A, Casarotto S, et al. A fast and general method to empirically estimate the complexity of brain responses to transcranial and intracranial stimulations. *Brain Stimul*. 2019;12(5):1280-1289. doi:10.1016/j.brs.2019.05.013
6. Arena A, Comolatti R, Thon S, Casali AG, Storm JF. General anesthesia disrupts complex cortical dynamics in response to intracranial electrical stimulation in rats. *Eneuro*. 2021;8(4):ENEURO.0343-20.2021. doi:10.1523/eneuro.0343-20.2021
7. Arena A, Juel BE, Comolatti R, Thon S, Storm JF. Capacity for consciousness under ketamine anaesthesia is selectively associated with activity in posteromedial cortex in rats. *Neurosci Conscious*. 2022;2022(1):niac004. doi:10.1093/nc/niac004
8. Mofakham S, Fry A, Adachi J, et al. Electrocorticography reveals thalamic control of cortical dynamics following traumatic brain injury. *Commun Biology*. 2021;4(1):1210. doi:10.1038/s42003-021-02738-2
9. Huang Y, Hajnal B, Entz L, et al. Intracortical Dynamics Underlying Repetitive Stimulation Predicts Changes in Network Connectivity. *J Neurosci*. 2019;39(31):6122-6135. doi:10.1523/jneurosci.0535-19.2019
10. Keller CJ, Huang Y, Herrero JL, et al. Induction and quantification of excitability changes in human cortical networks. *J Neurosci*. 2018;38(23):1088-17. doi:10.1523/jneurosci.1088-17.2018
11. Siddiqi SH, Kording KP, Parvizi J, Fox MD. Causal mapping of human brain function. *Nat Rev Neurosci*. Published online 2022:1-15. doi:10.1038/s41583-022-00583-8
12. Silverstein BH, Asano E, Sugiura A, Sonoda M, Lee MH, Jeong JW. Dynamic tractography: Integrating cortico-cortical evoked potentials and diffusion imaging. *Neuroimage*. 2020;215:116763. doi:10.1016/j.neuroimage.2020.116763
13. Trebaul L, Deman P, Tuyisenge V, et al. Probabilistic functional tractography of the human cortex revisited. *Neuroimage*. 2018;181:414-429. doi:10.1016/j.neuroimage.2018.07.039
14. Lemaréchal JD, Jedynak M, Trebaul L, et al. A brain atlas of axonal and synaptic delays based on modelling of cortico-cortical evoked potentials. *Brain*. 2021;145(5):1653-1667. doi:10.1093/brain/awab362
15. Blooijs D van, Boom MA van den, Aar JF van der, et al. Developmental trajectory of transmission speed in the human brain. *Nat Neurosci*. Published online 2023:1-5. doi:10.1038/s41593-023-01272-0

16. Veit MJ, Kucyi A, Hu W, et al. Temporal order of signal propagation within and across intrinsic brain networks. *Proc National Acad Sci*. 2021;118(48):e2105031118. doi:10.1073/pnas.2105031118
17. Seguin C, Jedynak M, David O, Mansour S, Sporns O, Zalesky A. Communication dynamics in the human connectome shape the cortex-wide propagation of direct electrical stimulation. *Neuron*. Published online 2023. doi:10.1016/j.neuron.2023.01.027
18. Smith EH, Liou J you, Merricks EM, et al. Human interictal epileptiform discharges are bidirectional traveling waves echoing ictal discharges. *Elife*. 2022;11:e73541. doi:10.7554/elife.73541
19. Muller L, Chavane F, Reynolds J, Sejnowski TJ. Cortical travelling waves: mechanisms and computational principles. *Nat Rev Neurosci*. 2018;19(5):255-268. doi:10.1038/nrn.2018.20
20. Sato TK, Nauhaus I, Carandini M. Traveling Waves in Visual Cortex. *Neuron*. 2012;75(2):218-229. doi:10.1016/j.neuron.2012.06.029
21. Zhang H, Jacobs J. Traveling Theta Waves in the Human Hippocampus. *J Neurosci*. 2015;35(36):12477-12487. doi:10.1523/jneurosci.5102-14.2015
22. Leibold C, Monsalve-Mercado MM. Traveling Theta Waves and the Hippocampal Phase Code. *Sci Rep-uk*. 2017;7(1):7678. doi:10.1038/s41598-017-08053-3
23. Muller L, Reynaud A, Chavane F, Destexhe A. The stimulus-evoked population response in visual cortex of awake monkey is a propagating wave. *Nat Commun*. 2014;5(1):3675. doi:10.1038/ncomms4675
24. Zhang H, Watrous AJ, Patel A, Jacobs J. Theta and Alpha Oscillations Are Traveling Waves in the Human Neocortex. *Neuron*. 2018;98(6):1269-1281.e4. doi:10.1016/j.neuron.2018.05.019
25. Davis ZW, Muller L, Martinez-Trujillo J, Sejnowski T, Reynolds JH. Spontaneous travelling cortical waves gate perception in behaving primates. *Nature*. 2020;587(7834):432-436. doi:10.1038/s41586-020-2802-y
26. Muller L, Piantoni G, Koller D, Cash SS, Halgren E, Sejnowski TJ. Rotating waves during human sleep spindles organize global patterns of activity that repeat precisely through the night. *Elife*. 2016;5:e17267. doi:10.7554/elife.17267
27. Khodagholy D, Gelinas JN, Thesen T, et al. NeuroGrid: recording action potentials from the surface of the brain. *Nat Neurosci*. 2015;18(2):310-315. doi:10.1038/nn.3905
28. Tchoe Y, Bourhis AM, Cleary DR, et al. Human brain mapping with multithousand-channel PtNRGrids resolves spatiotemporal dynamics. *Sci Transl Med*. 2022;14(628):eabj1441. doi:10.1126/scitranslmed.abj1441
29. Paulk AC, Yang JC, Cleary DR, et al. Microscale Physiological Events on the Human Cortical Surface. *Cereb Cortex*. 2021;31(8):3678-3700. doi:10.1093/cercor/bhab040
30. Kundu B, Davis TS, Philip B, et al. A systematic exploration of parameters affecting evoked intracranial potentials in patients with epilepsy. *Brain Stimul*. 2020;13(5):1232-1244. doi:10.1016/j.brs.2020.06.002
31. Davis TS, Caston RM, Philip B, et al. LeGUI: A Fast and Accurate Graphical User Interface for Automated Detection and Anatomical Localization of Intracranial Electrodes. *Front Neurosci-switz*. 2021;15:769872. doi:10.3389/fnins.2021.769872
32. Feinsinger A, Pouratian N, Ebadi H, et al. Ethical commitments, principles, and practices guiding intracranial neuroscientific research in humans. *Neuron*. 2022;110(2):188-194. doi:10.1016/j.neuron.2021.11.011

33. Fan L, Li H, Zhuo J, et al. The Human Brainnetome Atlas: A New Brain Atlas Based on Connectional Architecture. *Cereb Cortex*. 2016;26(8):3508-3526. doi:10.1093/cercor/bhw157
34. Matsumoto R, Kunieda T, Nair D. Single pulse electrical stimulation to probe functional and pathological connectivity in epilepsy. *Seizure*. 2017;44:27-36. doi:10.1016/j.seizure.2016.11.003
35. Lega B, Dionisio S, Flanigan P, et al. Cortico-cortical evoked potentials for sites of early versus late seizure spread in stereoelectroencephalography. *Epilepsy Res*. 2015;115:17-29. doi:10.1016/j.eplepsyres.2015.04.009
36. Cornblath EJ, Lucas A, Armstrong C, et al. Quantifying trial-by-trial variability during cortico-cortical evoked potential mapping of epileptogenic tissue. *Epilepsia*. Published online 2023. doi:10.1111/epi.17528
37. Smith RJ, Hays MA, Kamali G, et al. Stimulating native seizures with neural resonance: a new approach to localize the seizure onset zone. *Brain*. 2022;145(11):3886-3900. doi:10.1093/brain/awac214
38. Mercier MR, Dubarry AS, Tadel F, et al. Advances in human intracranial electroencephalography research, guidelines and good practices. *Neuroimage*. 2022;260:119438. doi:10.1016/j.neuroimage.2022.119438
39. Rolston JD, Gross RE, Potter SM. Common Median Referencing for Improved Action Potential Detection with Multielectrode Arrays. *2009 Annu Int Conf Ieee Eng Medicine Biology Soc*. 2009;2009:1604-1607. doi:10.1109/iembs.2009.5333230
40. Prime D, Rowlands D, O'Keefe S, Dionisio S. Considerations in performing and analyzing the responses of cortico-cortical evoked potentials in stereo-EEG. *Epilepsia*. 2018;59(1):16-26. doi:10.1111/epi.13939
41. Hays MA, Smith RJ, Haridas B, Coogan C, Crone NE, Kang JY. Effects of stimulation intensity on intracranial cortico-cortical evoked potentials: A titration study. *Clin Neurophysiol*. 2021;132(11):2766-2777. doi:10.1016/j.clinph.2021.08.008
42. Crocker B, Ostrowski L, Williams ZM, et al. Local and distant responses to single pulse electrical stimulation reflect different forms of connectivity. *Neuroimage*. 2021;237:118094. doi:10.1016/j.neuroimage.2021.118094
43. Miller KJ, Müller KR, Hermes D. Basis profile curve identification to understand electrical stimulation effects in human brain networks. *Plos Comput Biol*. 2021;17(9):e1008710. doi:10.1371/journal.pcbi.1008710
44. Crowther LJ, Brunner P, Kapeller C, et al. A quantitative method for evaluating cortical responses to electrical stimulation. *J Neurosci Meth*. 2019;311:67-75. doi:10.1016/j.jneumeth.2018.09.034
45. Prime D, Woolfe M, Rowlands D, O'Keefe S, Dionisio S. Comparing connectivity metrics in cortico-cortical evoked potentials using synthetic cortical response patterns. *J Neurosci Meth*. 2020;334:108559. doi:10.1016/j.jneumeth.2019.108559
46. Behrens TEJ, Berg HJ, Jbabdi S, Rushworth MFS, Woolrich MW. Probabilistic diffusion tractography with multiple fibre orientations: What can we gain? *Neuroimage*. 2007;34(1):144-155. doi:10.1016/j.neuroimage.2006.09.018
47. Charlebois CM, Anderson DN, Johnson KA, et al. Patient-specific structural connectivity informs outcomes of responsive neurostimulation for temporal lobe epilepsy. *Epilepsia*. 2022;63(8):2037-2055. doi:10.1111/epi.17298

48. Fischl B. FreeSurfer. *Neuroimage*. 2011;62(2):774-781. doi:10.1016/j.neuroimage.2012.01.021
49. Liou J you, Smith EH, Bateman LM, et al. Multivariate regression methods for estimating velocity of ictal discharges from human microelectrode recordings. *J Neural Eng*. 2017;14(4):044001. doi:10.1088/1741-2552/aa68a6
50. Waskom M. seaborn: statistical data visualization. *J Open Source Softw*. 2021;6(60):3021. doi:10.21105/joss.03021
51. Anderson TW, Darling DA. Asymptotic Theory of Certain "Goodness of Fit" Criteria Based on Stochastic Processes. *Ann Math Statistics*. 1952;23(2):193-212. doi:10.1214/aoms/1177729437
52. Benjamini Y, Hochberg Y. Controlling the False Discovery Rate: A Practical and Powerful Approach to Multiple Testing. *J Royal Statistical Soc Ser B Methodol*. 1995;57(1):289-300. doi:10.1111/j.2517-6161.1995.tb02031.x
53. Davis ZW, Benigno GB, Fletterman C, et al. Spontaneous traveling waves naturally emerge from horizontal fiber time delays and travel through locally asynchronous-irregular states. *Nat Commun*. 2021;12(1):6057. doi:10.1038/s41467-021-26175-1
54. Anderson DN, Charlebois CM, Smith EH, Arain AM, Davis TS, Rolston JD. Probabilistic comparison of gray and white matter coverage between depth and surface intracranial electrodes in epilepsy. *Sci Rep-uk*. 2021;11(1):24155. doi:10.1038/s41598-021-03414-5
55. Prime D, Woolfe M, O'Keefe S, Rowlands D, Dionisio S. Quantifying volume conducted potential using stimulation artefact in cortico-cortical evoked potentials. *J Neurosci Meth*. 2020;337:108639. doi:10.1016/j.jneumeth.2020.108639
56. Bernabei JM, Li A, Revell AY, et al. Quantitative approaches to guide epilepsy surgery from intracranial EEG. *Brain*. Published online 2023. doi:10.1093/brain/awad007
57. Enatsu R, Gonzalez-Martinez J, Bulacio J, et al. Connections of the limbic network: A corticocortical evoked potentials study. *Cortex*. 2015;62:20-33. doi:10.1016/j.cortex.2014.06.018
58. Mégevand P, Groppe DM, Bickel S, et al. The Hippocampus and Amygdala Are Integrators of Neocortical Influence: A CorticoCortical Evoked Potential Study. *Brain Connectivity*. 2017;7(10):648-660. doi:10.1089/brain.2017.0527
59. Guo Z, Zhao B, Hu W, et al. Effective connectivity among the hippocampus, amygdala, and temporal neocortex in epilepsy patients: A cortico-cortical evoked potential study. *Epilepsy Behav*. 2021;115:107661. doi:10.1016/j.yebeh.2020.107661
60. Halgren M, Ulbert I, Bastuji H, et al. The generation and propagation of the human alpha rhythm. *Proc National Acad Sci*. 2019;116(47):23772-23782. doi:10.1073/pnas.1913092116